Energy barriers for bit-encoding states based on 360° domain walls in ultrathin ferromagnetic nanorings

C. B. Muratov, V. V. Osipov, and E. Vanden-Eijnden

Citation: Journal of Applied Physics **117**, 17D118 (2015); doi: 10.1063/1.4914341
View online: http://dx.doi.org/10.1063/1.4914341
View Table of Contents: http://scitation.aip.org/content/aip/journal/jap/117/17?ver=pdfcov
Published by the AIP Publishing

Energy barriers for bit-encoding states based on 360° domain walls in ultrathin ferromagnetic nanorings

C. B. Muratov,[1,a)] V. V. Osipov,[2] and E. Vanden-Eijnden[3]
[1]*Department of Mathematical Sciences, New Jersey Institute of Technology, Newark, New Jersey 07102, USA*
[2]*Intelligent Systems Division, D&SH Branch, NASA Ames Research Center, MS 269-1, Moffett Field, California 94035, USA*
[3]*Courant Institute of Mathematical Sciences, New York University, New York, New York 10012, USA*

(Presented 7 November 2014; received 20 September 2014; accepted 2 November 2014; published online 10 March 2015)

A numerical thermal stability study of the bit-encoding states in a proposed multi-level magnetic storage element based on an ultrathin ferromagnetic nanoring is presented. The material parameters and the ring dimensions for which there are five distinct metastable magnetization configurations separated by energy barriers exceeding $50k_BT$ at room temperature are identified. The results are obtained, using the string method for the study of rare events to locate the transition states separating the metastable states and to identify the most likely thermally activated pathways. © *2015 AIP Publishing LLC*. [http://dx.doi.org/10.1063/1.4914341]

I. INTRODUCTION

Ferromagnetic nanorings have long been considered as promising storage elements for magnetoresistive random access memory (MRAM).[1–9] In the simplest device concept, one bit of information is encoded by the polarity of the vortex state in a ring. It has been realized that switching between the two vortex directions may present difficulties due to high current densities that may be required.[5–7,10,11] At the same time, while vortices are always energetically preferred, in ultrathin ferromagnetic nanorings, they coexist with the long-lived metastable magnetization configurations, such as the onion and the twisted states, which belong to a different topological class.[7,12,13] Persistence of these configurations is due to the fact that by topological reasons the magnetization is required to go out of plane in order for a transition to the vortex state to occur. Such fluctuations are strongly penalized in ultrathin ferromagnetic rings.[14]

The considerations above motivated a MRAM design concept, in which a bit is encoded by the magnetization configurations containing a 360° domain wall.[3,9] The presence of a 360° domain wall in an otherwise vortex-like configuration ensures that the configuration has topological degree zero.[9] In this concept, the magnetization vector always remains in the film plane, and the configurations are manipulated by the circular Oersted field created by a current passing through the ring center[6,9] (see Fig. 1). Note that the feasibility of creating and manipulating 360° domain walls in ferromagnetic nanorings using a perpendicular current was recently confirmed experimentally.[15]

In order for a MRAM cell design to be competitive with the existing non-volatile random access storage technologies,[16–18] it is necessary to minimize the dimensions of the individual storage cell while maintaining robustness of the bit-encoding magnetization configurations against thermal noise.[19,20] Also, it is desirable to reduce the complexity of the accessible metastable states to ensure reliable switching. Therefore, one needs to look for a design specification in which only a few easily distinguishable metastable magnetization configurations separated by barriers exceeding around $50k_BT$ are present.

In this paper, we present a micromagnetic study of thermal stability of the bit-encoding states in the case of an ultrathin ferromagnetic nanoring-based MRAM cell which uses 360° domain walls. We used the string method[21] to find the transition states between the metastable configurations (see also Ref. 22 for another possible numerical approach). These transition states are saddle points along the minimum energy path (MEP) connecting two metastable configurations (local energy minimizers). The topology of the network of MEPs

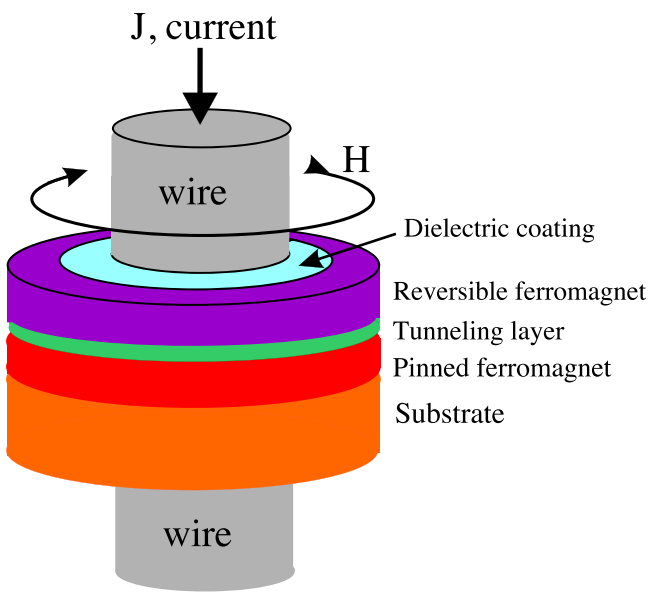

FIG. 1. The schematics of a ferromagnetic nanoring based MRAM cell (from Ref. 9).

a)Author to whom correspondence should be addressed. Electronic mail: muratov@njit.edu.

indicates which one-step thermally activated transitions are possible, and the height ΔE of the energy barrier between a metastable configuration and a transition state gives an estimate of the rate J of this transition via the Arrhenius law: $J \simeq J_0 e^{-\Delta E/k_B T}$, where J_0 is a prefactor which depends on the details of the dynamics but not on temperature to the leading order (for details, see Refs. 23–25). This thereby allows us to estimate the stability of the magnetic ring against thermal fluctuations.

Specifically, we identified a parameter regime which reliably produces five types of metastable magnetization configurations which are well distinguished by a magnetoresistive signal measurement. Our results indicate that the storage elements using rings made of 5 nm-thick epitaxial cobalt films may be scaled down to about 360 nm outer and 240 nm inner diameters at room temperature. Further reduction in the ring size, however, may result in an unacceptable deterioration of thermal stability.

II. MODEL

Our starting point is the micromagnetic energy[26]

$$E(\mathbf{M}) = \int_\Omega \left(\frac{A}{2M_s^2} |\nabla \mathbf{M}|^2 + \frac{K}{2M_s^4} M_1^2 M_2^2 \right) d^3 r + \frac{1}{2} \int_{\mathbb{R}^3} \int_{\mathbb{R}^3} \frac{\nabla \cdot \mathbf{M}(\mathbf{r}) \, \nabla \cdot \mathbf{M}(\mathbf{r}')}{|\mathbf{r} - \mathbf{r}'|} \, d^3 r \, d^3 r', \quad (1)$$

where the three terms in the right-hand side are the exchange, the four-fold in-plane anisotropy typical of ultrathin epitaxial films,[27] and the stray field contributions, respectively, $\Omega \subset \mathbb{R}^3$ is the domain occupied by the ferromagnetic material, $\mathbf{M} = (M_1, M_2, M_3)$ is the magnetization vector, such that $|\mathbf{M}|$ equals the saturation magnetization M_s in Ω and zero outside, A is the exchange constant, K is the anisotropy constant, and the last term is understood in the distributional sense. In the case of an ultrathin ring of thickness d (more precisely, when $d \ll 7l$, where $l = (A/4\pi M_s^2)^{1/2}$ is the exchange length[26]) and of soft ferromagnetic material (more precisely, when the quality factor $Q = (K/4\pi M_s^2)^{1/2} \ll 1$), we can further reduce the energy in (1) by assuming that the magnetization does not vary appreciably across the film thickness and that the magnetization vector lies almost entirely in the film plane,[28–31] i.e., that $\mathbf{M}(x, y, z) = M_s u(d^2 - 4z^2)\chi(x, y)(-\sin\theta(x, y), \cos\theta(x, y), 0)$, where χ is the characteristic function of the annulus of inner radius R_1 and outer radius R_2 in the plane and $u(t)$ is the Heaviside step function. Here, θ is the angle that the in-plane component of the magnetization vector makes with the y-axis (an easy axis). Then, to the leading order in d, we obtain the following reduced energy:

$$\frac{E(\mathbf{M})}{E_0} \simeq \int_{\mathbb{R}^2} \left(\frac{1}{2} \chi^2 |\nabla \theta|^2 + \frac{1}{2} \chi^4 \sin^2\theta \cos^2\theta \right) d^2 r + \frac{\nu}{8\pi} \int_{\mathbb{R}^2} \int_{\mathbb{R}^2} \frac{\partial_y (\chi(\mathbf{r}) \cos\theta(\mathbf{r})) - \partial_x (\chi(\mathbf{r}) \sin\theta(\mathbf{r}))}{|\mathbf{r} - \mathbf{r}'|} \times \left(\partial_y (\chi(\mathbf{r}') \cos\theta(\mathbf{r}')) - \partial_x (\chi(\mathbf{r}') \sin\theta(\mathbf{r}')) \right) d^2 r \, d^2 r', \quad (2)$$

where $E_0 = Ad = 4\pi M_s^2 l^2 d$ is the unit of energy, $\nu = 4\pi M_s^2 d/(AK)^{1/2} = d/(lQ^{1/2})$ is the dimensionless thin film parameter,[30] and in writing the dimensionless energy functional in the right-hand side of (2) the unit of length was chosen to be the Bloch wall width $L = (A/K)^{1/2}$. It is also necessary to mollify the characteristic function χ of the annulus to avoid divergent integrals from the boundary of the ring in the last term in (2). We, therefore, take $\chi(\mathbf{r}) = (1 + \exp(b^{-1}(|\mathbf{r}| - R_2)))^{-1}(1 + \exp(b^{-1}(R_1 - |\mathbf{r}|)))^{-1}$, where b is a cutoff length, which should be chosen of order d/L (in the new units).

Note that since the divergence as $b \to 0$ near the boundary is logarithmic (compare with Ref. 29), the energy only weakly depends on the specific choice of b. Therefore, in practice, b can be set to the numerical discretization length. On the other hand, the introduction of a mollified characteristic function χ permits the use of a square discretization grid for the part of the plane containing the annulus, combined with optimal finite difference grids to compute the stray field, and, thus, to adapt a previously developed highly efficient code for rectangular domains[30] to films of arbitrary two-dimensional shapes. This approach also has an advantage of not being sensitive to the misalignment of the material boundary with the numerical grid and was used by us previously in Refs. 9, 32, and 33. Numerically, we use the $L^2(\mathbb{R}^2; \chi d^2 r)$ gradient flow dynamics (see Eq. (12) in Ref. 32) generated by the energy in the right-hand side of (2) to obtain local minimizers of the energy (discretized in space, using centered differences with $\Delta x = 0.25$, and explicit in time Euler scheme with $\Delta t = 0.0125$ on a square 129×129 grid extended by 6 layers of Zolotarev grid in each direction[30]). We then call this solver from the simplified string method algorithm[34] to compute the saddle points of the energy.

III. RESULTS

Previous numerical studies showed that epitaxial ultrathin ferromagnetic nanorings exhibit a complex array of low energy metastable configurations with topological degree zero.[32,33] We found that in sufficiently narrow rings (i.e., when $R_2 - R_1 \lesssim R_1$), those reduce to three basic types of configurations: two 360° domain wall states, two twisted onion states, and one onion state. These are shown in Figs. 2(a)–2(c), respectively, for $R_1 = 10$, $R_2 = 15$, and $\nu = 5$. The choice of the dimensionless parameters was determined by the reproducibility of the above configurations, while ensuring sufficiently high energy barriers between them for the smallest outer ring radius R_2. This puts competing constraints on the dimensionless parameters: larger values of ν or smaller values of R_1 produce more metastable configurations,[32,33] while smaller values of ν or larger values of R_1 reduce the barrier heights.

Note that by symmetry there are 8 variants of the 360° domain wall states (4 rotations and 2 reflections), 8 twisted onion states (4 rotations and 2 reflections), and 4 onion states (4 rotations). However, since rotations do not affect the magnetoresistive readout from the MRAM cell (assuming that the reference layer of the magnetic tunnel junction is in the

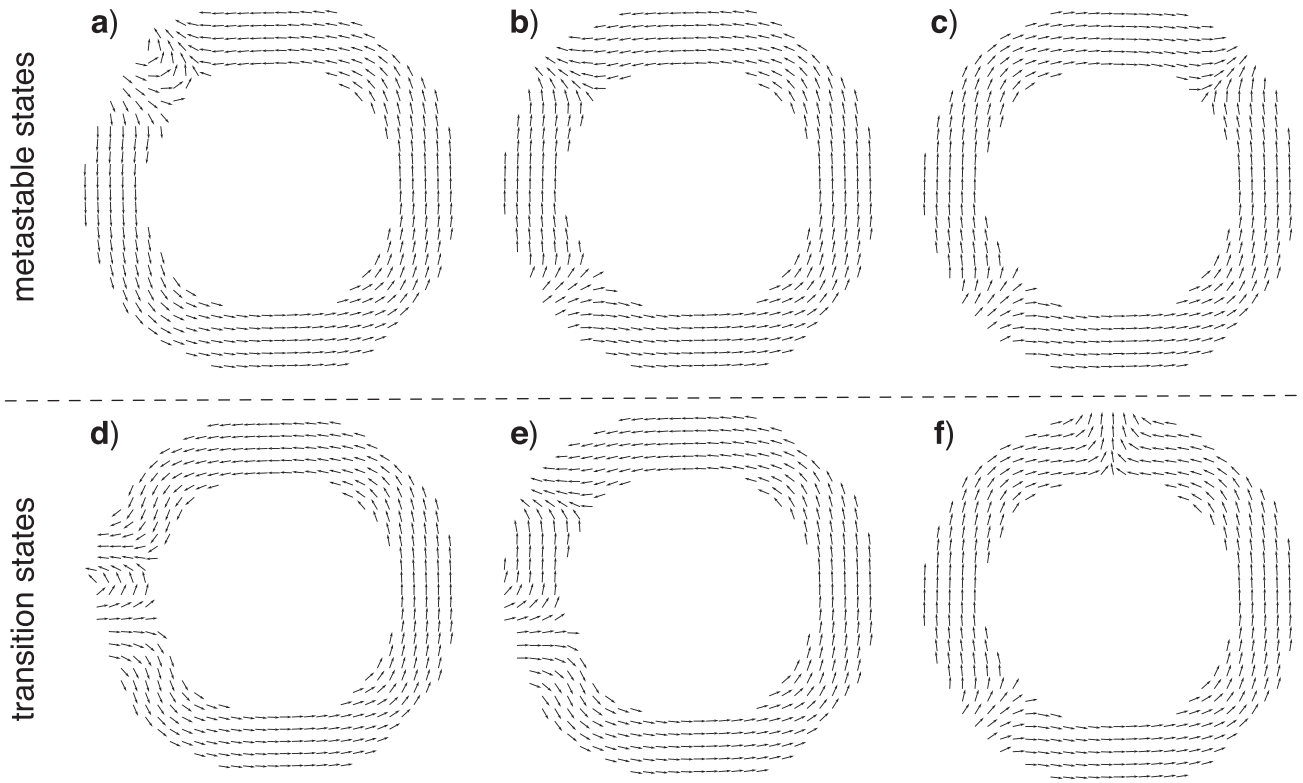

FIG. 2. Three main types of the metastable states ((a)–(c)) and the transition states ((d)–(f)) in a narrow ring. Results of the numerical study of (2) for $R_1 = 10$, $R_2 = 15$, and $\nu = 5$. In all the panels, the vector field $(-\sin\theta, \cos\theta)$ is shown.

vortex state), the first two types correspond to two distinct states each, while the latter corresponds to one state. In all, there are five distinct magnetization states that may be stored and read by the cell. These configurations may be used for multi-level encoding in a single MRAM cell, with 5 distinct storable states available. Alternatively, just the two 360° domain wall states with the opposite polarities (which have the highest magnetoresistive contrast) may be used to encode the two bits. The latter represents the original proposal of Ref. 9 for the considered design. We found that the 360° domain wall states have the lowest energy among all the metastable configurations and thus represent the ground states of the system within the considered topological class.

We next used the obtained metastable states as the endpoint configurations of the string method algorithm to search for the transition states. The string was initialized, using linear interpolation between the endpoint configurations with 41 string discretization points. The string was then evolved to yield the MEP, along which the state of maximal energy is a transition state. The MEPs from and to the twisted onion state are shown in Fig. 3. The saddle point configuration for the path from the twisted onion to a 360° domain wall state from Fig. 3(a) is shown in Fig. 2(e), with the barrier height $\Delta E \simeq 1.86E_0$ for the forward transition and the barrier height $\Delta E \simeq 3.57E_0$ for the backward transition. Similarly, the saddle point configuration for the path from the twisted onion to the onion state from Fig. 3(b) is shown in Fig. 2(f), with the barrier height $\Delta E \simeq 3.92E_0$ for the forward transition and the barrier height $\Delta E \simeq 3.34E_0$ for the backward transition. From these results, we can conclude that the transition from the 360° domain wall state to the same state, but with the opposite polarity, would proceed via the twisted onion state, followed by the onion state [Fig. 2(a) → Fig. 2(e) → Fig. 2(b) → Fig. 2(f) → Fig. 2(c)], followed by the twisted onion state of the opposite polarity, with the barrier height of $\Delta E \simeq 5.61E_0$. In all the cases, transitions between different metastable configurations appear to occur by a 45° motion of a single 180° wall head.

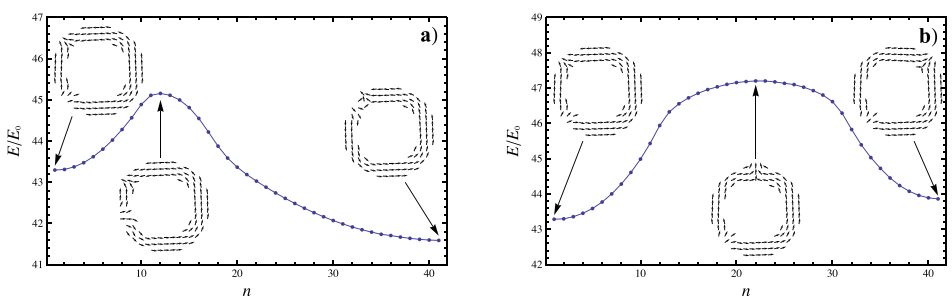

FIG. 3. The energy of the magnetization configurations on the string connecting a twisted onion with a 360° domain wall state (a) or an onion state (b). Same parameters as in Fig. 2.

Looking at the results in Fig. 3, one may be lead to a conclusion that the transition from a 360° domain wall state in Fig. 2(a) to its 90° counterclockwise rotation should occur via the formation of a twisted onion state from Fig. 2(b). However, our further analysis, using the string method, showed that there is also a direct pathway via a saddle point configuration in Fig. 2(d), with the slightly lower barrier height $\Delta E \simeq 3.40E_0$. We also found an apparent local minimum of the energy in the form of a 360° domain wall which looks like a 45° rotation of the configuration in Fig. 2(a). However, this configuration has a very low $(\Delta E \lesssim 0.02E_0)$ energy barrier in the direction of the state in Fig. 2(a) and thus is unstable for realistic levels of thermal noise.

Let us now see what the results obtained above imply for a practical implementation of a ferromagnetic nanoring-based MRAM cell. Assuming that the ring is made of cobalt, we set $M_s = 1400\,\mathrm{emu/cm^3}$, $A = 2.8 \times 10^{-6}\,\mathrm{erg/cm}$, and $K = 2 \times 10^6\,\mathrm{erg/cm^3}$, cf. Refs. 27 and 35. This yields the exchange length $l \simeq 3.37\,\mathrm{nm}$, the Bloch wall thickness $L \simeq 12\,\mathrm{nm}$, and the quality factor $Q \simeq 0.08$, as in Ref. 9. Then the parameters used in our simulations would correspond to a film of thickness $d \simeq 5\,\mathrm{nm}$, inner radius $R_1 \simeq 120\,\mathrm{nm}$, and outer radius $R_2 \simeq 180\,\mathrm{nm}$. In turn, with the working temperature of 65 °C, the unit of energy becomes $E_0 \simeq 30k_BT$. This implies that the energy barriers for all the considered metastable states in a 5-level MRAM cell narrowly exceed $50k_BT$, indicating that the proposed design is indeed robust with respect to thermal noise. In turn, a two-level MRAM cell using only two 360° domain wall states would have the barrier of about $170k_BT$, allowing for some further reduction of the cell size.

IV. CONCLUSION

In conclusion, we presented a multi-level extension of the ferromagnetic nanoring-based MRAM cell design proposed in Ref. 9 and demonstrated its robustness with respect to thermal noise for cobalt rings down to 360 nm in diameter. We believe that the parameter regime identified in our study should be close to optimal, since it satisfies a set of rather tight competing constraints under the requirement of minimizing the overall cell size.

ACKNOWLEDGMENTS

The work of C.B.M. was supported by NSF via Grant Nos. DMS-0908279 and DMS-1313687. E. V.-E. was supported in part by NSF Grant No. DMS-0708140 and ONR Grant No. N00014-11-1-0345.

[1]J.-G. Zhu, Y. Zheng, and G. A. Prinz, J. Appl. Phys. **87**, 6668 (2000).
[2]X. Zhu and J.-G. Zhu, IEEE Trans. Magn. **39**, 2854 (2003).
[3]C. A. Ross and F. J. Castano, "Magnetic memory elements using 360° walls," U.S. patent 6,906,369 B2 (2005).
[4]T. J. Hayward, J. Llandro, R. B. Balsod, J. A. C. Bland, F. J. Castaño, D. Morecroft, and C. A. Ross, Appl. Phys. Lett. **89**, 112510 (2006).
[5]M. T. Moneck and J.-G. Zhu, J. Appl. Phys. **99**, 08H709 (2006).
[6]K. Martens, D. L. Stein, and A. D. Kent, Phys. Rev. B **73**, 054413 (2006).
[7]C. A. F. Vaz, T. J. Hayward, J. Llandro, F. Schackert, D. Morecroft, J. A. C. Bland, M. Kläui, M. Laufenberg, D. Backes, U. Rudiger *et al.*, J. Phys. -Condens. Matter **19**, 255207 (2007).
[8]X. F. Han, Z. C. Wen, and H. X. Wei, J. Appl. Phys. **103**, 07E933 (2008).
[9]C. B. Muratov and V. V. Osipov, IEEE Trans. Magn. **45**, 3207 (2009).
[10]G. D. Chaves-O'Flynn, K. Xiao, D. L. Stein, and A. D. Kent, J. Appl. Phys. **103**, 07D917 (2008).
[11]G. D. Chaves-O'Flynn, A. D. Kent, and D. L. Stein, Phys. Rev. B **79**, 184421 (2009).
[12]F. J. Castaño, C. A. Ross, C. Frandsen, A. Eilez, D. Gil, H. I. Smith, M. Redjdal, and F. B. Humphrey, Phys. Rev. B **67**, 184425 (2003).
[13]F. J. Castaño, C. A. Ross, A. Eilez, W. Jung, and C. Frandsen, Phys. Rev. B **69**, 144421 (2004).
[14]G. D. Chaves-O'Flynn, D. Bedau, E. Vanden-Eijnden, A. D. Kent, and D. L. Stein, IEEE Trans. Magn. **46**, 2272 (2010).
[15]T. Yang, N. R. Pradhan, A. Goldman, A. S. Licht, Y. Li, M. Kemei, M. T. Tuominen, and K. E. Aidala, Appl. Phys. Lett. **98**, 242505 (2011).
[16]W. Zhao, L. Torres, Y. Guillemenet, L. V. Cargnini, Y. Lakys, J.-O. Klein, D. Ravelosonsa, G. Sassatelli, and C. Chappert, in *Proceedings of the 21st edition of the Great Lakes Symposium on VLSI (GLSVLSI'11)* (ACM, New York, NY, USA, 2011), pp. 431–436.
[17]E. Eleftheriou, R. Haas, J. Jelitto, M. Lantz, and H. Pozidis, IEEE Data Eng. Bull. **33**, 4 (2010).
[18]Y. Fujisaki, IEICE Electron. Express **9**, 908 (2012).
[19]S. Tehrani, J. M. Slaughter, M. Deherrera, B. N. Engel, N. D. Rizzo, J. Salter, M. Durlam, R. W. Dave, J. Janesky, B. Butcher *et al.*, Proc. IEEE **91**, 703 (2003).
[20]J.-G. Zhu, Proc. IEEE **96**, 1786 (2008).
[21]W. E, W. Ren, and E. Vanden-Eijnden, Phys. Rev. B. **66**, 052301 (2002).
[22]E. Vanden-Eijnden and M. Heymann, J. Chem. Phys. **128**, 061103 (2008).
[23]P. Hänggi, P. Talkner, and M. Borkovec, Rev. Mod. Phys. **62**, 251 (1990).
[24]W. E and E. Vanden-Eijnden, Annu. Rev. Phys. Chem. **61**, 391 (2010).
[25]W. E, W. Ren, and E. Vanden-Eijnden, J. Appl. Phys. **93**, 2275 (2003).
[26]A. Hubert and R. Schäfer, *Magnetic Domains* (Springer, Berlin, 1998).
[27]B. Heinrich and J. F. Cochran, Adv. Phys. **42**, 523 (1993).
[28]A. DeSimone, R. V. Kohn, S. Müller, and F. Otto, in *ICIAM 99 (Edinburgh)* (Oxford University Press, 2000), pp. 175–190.
[29]R. V. Kohn and V. V. Slastikov, Arch. Ration. Mech. Anal. **178**, 227 (2005).
[30]C. B. Muratov and V. V. Osipov, J. Comput. Phys. **216**, 637 (2006).
[31]C. B. Muratov and V. V. Osipov, J. Appl. Phys. **104**, 053908 (2008).
[32]G. D. Chaves-O'Flynn and C. B. Muratov, IEEE Trans. Magn. **49**, 3125 (2013).
[33]G. D. Chaves-O'Flynn and C. B. Muratov, in *American Physical Society March Meeting*, March 18–22, 2013, Abstract No. H1.172.
[34]W. E, W. Ren, and E. Vanden-Eijnden, J. Chem. Phys. **126**, 164103 (2007).
[35]S. P. Li, D. Peyrade, M. Natali, A. Lebib, Y. Chen, U. Ebels, L. D. Buda, and K. Ounadjela, Phys. Rev. Lett. **86**, 1102 (2001).